JOURNAL OF RAMAN SPECTROSCOPY
J. Raman Spectrosc. 2004; **35**: 504–514
Published online in Wiley InterScience (www.interscience.wiley.com). DOI: 10.1002/jrs.1175

JRS

Mineralogy of a Martian meteorite as determined by Raman spectroscopy

Alian Wang,* Karla Kuebler, Bradley Jolliff and Larry A. Haskin

Department of Earth and Planetary Sciences and McDonnell Center for Space Sciences, Washington University, St. Louis, Missouri 63130, USA

Received 6 June 2003; Accepted 12 November 2003

Using the Raman point-count procedure that we anticipate using in planetary surface exploration, we have identified and characterized the major, minor and trace mineral phases in rock chips of a Martian meteorite, EETA 79001. Raman spectra are shown for pyroxene, olivine, maskelynite (shocked, isotropized feldspar), chromite, magnetite, ilmenite, ulvöspinel, pyroxferroite, merrillite, apatite, anatase, an Fe sulfide, calcite and hematite. Raman spectra provide information on compositional variations of pyroxene, olivine and Fe–Ti–Cr oxides and modal proportions of the rock. The maskelynite-free mineral mode obtained on rough rock surfaces is consistent with modes obtained by optical microscopy on a thin section of lithology A of this meteorite. Compositions and variations in compositions of major silicate minerals (pyroxene and olivine) on the basis of Raman peak positions are consistent with those obtained in previous studies by electron probe microanalysis. The variations in composition of the silicate minerals represent different stages of crystallization during the formation of this rock near the Martian surface. Copyright © 2004 John Wiley & Sons, Ltd.

KEYWORDS: Mars; Martian meteorite; planetary mineralogy; solar system exploration

INTRODUCTION

We may expect several missions to land on Mars in this decade.[1,2] During planetary surface exploration, a high priority is to identify and characterize surface materials, especially to do definitive mineralogy, in order to understand Mars's evolutionary history. We are also concerned with determination of mineral chemical composition and estimation of the relative proportions of different minerals in a rock or soil. Because we know the chemical and physical conditions under which individual minerals form, we will learn about past Martian environmental conditions from such detailed mineralogical information. The mineralogical record in surface rocks is expected to reach back in Martian history from relatively recent alteration of rock surfaces to past stream and lake environments, potentially to hydrothermal settings within the upper martian crust and to the planet's early igneous chemical differentiation. With better knowledge of Mars' past and present environments, we can speculate more rationally on the possible development of life on that planet.

*Correspondence to: Alian Wang, Department of Earth and Planetary Sciences and McDonnell Center for Space Sciences, Washington University, St. Louis, Missouri 63130, USA.
E-mail: alianw@levee.wustl.edu
Contract/grant sponsor: NASA; Contract/grant number: NAG5-10703; NAG5-12114; NAG5-12684.

For the general characterization of minerals (including bound and unbounded H_2O) and biogenic phases (reduced carbon, PAHs, etc.) on the surface of Mars, we have been developing a miniaturized laser Raman spectrometer for *in situ* analyses—the Mars Microbeam Raman Spectrometer (MMRS).[3] We are also developing strategies to use Raman spectroscopy as a stand-alone technique or, even better, to be used synergistically with other *in situ* analytical methods in future planetary missions. Through studies of Martian meteorites and terrestrial analogs,[4,5] we are gaining experience regarding compositional and structural information that can be obtained on key mineral groups using *in situ* Raman measurements.[6–9] We are developing methods for determining mineral proportions in rocks or soils and identifying rock types from sets of closely spaced, rapidly acquired spectra.[10] We are studying how weathering and alteration affect the Raman and luminescence features of minerals and rocks,[11,12] and we are investigating Raman characteristics of biogenic organisms and their remains.[13,14] These studies form the scientific basis for *in situ* Planetary Raman spectroscopy,[15] and they are being done in parallel with instrument development towards a flight version of the MMRS.[16]

We can extensively characterize a target rock or soil using Raman spectroscopy. In particular, we propose to use a Raman point-count method.[10] In this method, the instrument scans across the target taking spectra at fixed intervals. At

each point sampled, we obtain definitive identification of the minerals from the spectrum; this includes minor and trace minerals as long as they are intercepted by the laser beam. We obtain chemical information for most minerals. We learn the mineral associations, i.e. which minerals usually or always form together in a microscopic location in the rock as it crystallizes or is later altered by the action of water. We estimate grain sizes for the major minerals. We determine the proportions of the major minerals. From the proportions and compositions of the major minerals, we can identify the type of rock. These properties can be determined on a rock or soil as it is encountered in the field, i.e. no sample preparation is needed.

In this paper, we present the results of a Raman point-count study on a Martian meteorite, EETA79001. We used a laboratory Raman system (HoloLab 5000, Kaiser Optical Systems) for this study. The point-count procedure allowed us to identify the major, minor and trace minerals in this Martian rock, determine the compositional features of major basaltic minerals and demonstrate how information on grain sizes and rock textures can be obtained. The current advanced brassboard[3] of the MMRS has similar spectral resolution and a detection sensitivity approaching ~40% of the laboratory system used in this study, so we expect results from the anticipated flight version of the MMRS that are similar in quality to those presented here.

EXPERIMENTAL

Sample

Martian meteorite EETA79001, the subject of this study, was found on the ice at the Elephant Moraine sampling site near Reckling Peak, Victoria Land, Antarctica, in 1979. It is one of a group of meteorites thought to be from Mars on the basis of glass inclusions that contain rare gas and nitrogen isotope compositions matching those of the Martian atmosphere[17] as determined by the Viking spacecraft.[18–20] It is a 'shergottite', a basaltic rock generally similar to the Martian meteorite Shergotty. It is rich in the mineral pyroxene and consists mainly of two related igneous lithologies (designated A and B) that are separated by an igneous or an impact-melt contact.[21,22] The two lithologies are related, but differ in texture and in mineral compositions and assemblages (i.e. the sets of different minerals that they contain). Pigeonite, augite and maskelynite (plagioclase made isotropic by shock due to impact) are the major minerals in both lithologies, but lithology A contains coarse crystals (xenocrysts or megacrysts) of olivine and orthopyroxene that are more magnesian than their counterparts in the finer grained basaltic matrix. The groundmass of lithology A has an average grain size of ~0.15 mm and the grains show no preferred orientation.[22] Lithology B is mineralogically similar to the groundmass of A, but is coarser (mean grain size ~0.35 mm) and represents a chemically more evolved composition (e.g. pyroxene compositions extend to higher Fe concentrations[22]). One rock chip (EETA79001,476) and a petrographic thin section (a polished rock slice mounted on glass) (TS442) from lithology A, and four rock chips (EETA79001,482) and a thin section (TS357) from lithology B were allocated to us for the Raman spectroscopic study. A thin section (TS530) was made from one of the rock chips of EETA79001,482 for further study by Raman spectroscopy, electron probe microanalysis and optical microscopy to understand better the lithology of this sample.

Procedure

The automated scanning stage of our HoloLab 5000 Raman system (Kaiser Optical Systems) was used for all of the Raman measurements reported here. Radiation of 632.8 nm from an He–Ne laser was used as the excitation source for most measurements; 532 nm radiation from a frequency-doubled Nd : YAG laser was used for a few. The Raman spectrometer has a spectral resolution of 4–5 cm^{-1}. The wavelength calibration was done by least-squares fitting to a set of standard Ne lines. The wavenumber accuracy is better than 0.5 cm^{-1} in the spectral region of interest; wavenumber reproducibility was checked using the Raman peak of an Si wafer each working day, and was better than ~0.3 cm^{-1} over several months. A 20× long-working-distance objective was used for all Raman measurements. It provides a condensed laser beam ~6 μm in diameter at the focal plane. All rock chips were measured using a Raman 'point-counting' procedure,[10] in which the excitation laser beam scans across the surface of an 'unprepared' rock chip (i.e., a chip with a rough, unpolished surface) and spectra will be taken at fixed intervals (e.g. every 100 μm). The MMRS will achieve this by moving the optical bench of the Raman probe along the surface of a rock; in the laboratory this was achieved by allowing the automated scanning stage to move the sample laterally beneath the laser beam.

Automatic focusing is an unnecessary complication for a flight Raman spectrometer, especially one to be deployed by a robotic arm. To simulate the use of the MMRS under field conditions, the laser beam was focused only at the starting point of each traverse and no focal adjustment was made before taking subsequent spectra. The sampled surface was thus slightly above or below the laser focal plane at most points because of the surface roughness of the rock. As a consequence, the signal-to-noise (S/N) ratio of many spectra is lower than would be the case for in-focus Raman measurements on thin sections. Also, the sampling volumes are somewhat increased. The peak positions in the spectra obtained by point-count measurements were determined by visually locating the symmetric center of each peak after baseline subtraction from the raw spectra. The precision of determining Raman peak positions by this method is estimated to be ±1 cm^{-1}.

In order to verify the compositional features derived from the point-count Raman data. Co-registered Raman in-focus

spectral measurements and electron microprobe analyses were made on individual mineral grains in three thin sections. A JEOL 733 Superprobe with a backscattered electron detector, three wavelength-dispersive spectrometers and an energy-dispersive spectrometer was used with Advanced Microbeam automation for the electron microprobe analyses. All analyses used an accelerating voltage of 15 kV; the beam current used was 30 nA for the olivine and pyroxene grains and 40 nA for the Fe–Ti–Cr oxides and the phosphates. The beam diameter was between 1 and 20 μm, depending on the grain size of the target and the objective of the analysis. We used a combination of silicate and oxide mineral standards. X-ray matrix corrections were based on a modified Armstrong (1988) CITZAF routine incorporated into the electron microprobe software. Table 1 shows typical compositions of major and minor mineral phases in this meteorite.

RESULTS AND DISCUSSION

Raman point-counting measurements were made on rough, broken surfaces of the rock chips (EETA79001,476 and 79001,482, Fig. 1) with surface relief on the order of about 1 mm. Four sets of point-count measurements were taken along linear traverses or on rectangular grids on the single rock chip of 79001,476 and seven sets were taken on four rock chips of 79001,482. A step size of 200 μm was used for two sets of the point counts, 50 μm for three of the linear traverses and 100 μm for the rest. The longest linear traverse covered ~12 mm of rock surface. We estimate that >95% of the measurements were made off-focus, as will be the case for on-planetary-surface measurements with the MMRS. Some 560 spectra were obtained from the rock chip of 79001,476 and 505 from the rock chips of 79001,482. The S/N ratios of the spectra vary from excellent to poor, but >99% of the points yielded spectra adequate for mineral identification.

Mineral identification and mineral modes

Our point-count study of Martian meteorite EETA79001 provides identification of all the known well crystalline minerals in the rock and provides accurate proportions of pyroxene and olivine, the two major crystalline phases. In a point-count Raman characterization of a rock or soil, our ability to observe all the different minerals in the rock depends on how many points are included in the scan and on how uniformly distributed the minerals are, so that our scan crosses a characteristic region of the rock. Some rocks are more homogeneous than others. The accuracy to which we determine the relative proportions of the major minerals depends on the number of points scanned; even 100 points are adequate for accurate determination of rock type. The accuracy with which we can determine the proportions of minor and trace minerals depends on the number of points, the homogeneity of their distribution within the rock and their relative Raman scattering cross-sections and grain sizes.

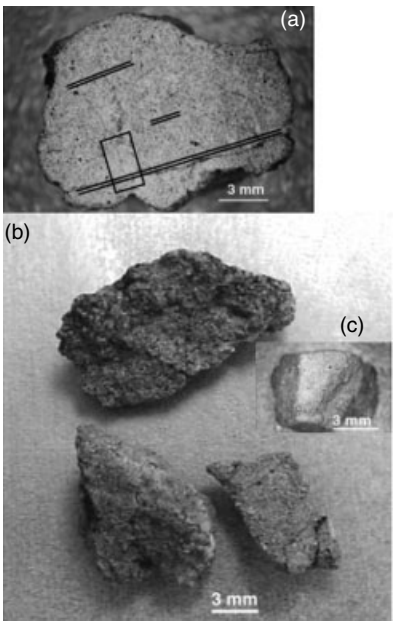

Figure 1. Rock chips of martian meteorite EETA79001 measured during this study: (a) EETA79001,476, showing the positions of the Raman point-counting traverses; (b) three chips of EETA79001,482, showing the roughness of the sample surfaces; (c) a fourth rock chip of EETA79001,482, on which calcite was detected, was later sliced to make thin section EETA79001,530. This meteorite is essentially a piece of basaltic lava, which is the most common type of lava on the Earth and also the Moon.

Spectral peaks from weaker scatterers such as most opaque minerals may, in some cases, be masked by those of stronger scatterers in multi-mineralic spectra, so we may expect that the proportions of weaker scatterers will be underestimated. We observe this in the study of EETA79001. This is especially true for the glassy maskelynite, the spectrum of which is almost always masked by the spectra of pyroxene or olivine. Maskelynite is produced when the mineral feldspar is shocked. When the feldspar is crystalline, its relative proportion is accurately determined, as we have shown in previous work.[10] Also, the proportion of opaque minerals in EETA79001 is greater than we observe in the spectra. The spectra of opaque minerals tend to be masked by those of pyroxene and olivine in out-of-focus spectra. The opposite is the case for the strongly scattering phosphate minerals apatite and merrillite. These minerals appear strongly, and in out-of-focus spectra in which they may even mask the spectra of major minerals. Hence, unlike the situation for major minerals, obtaining proportions of minor minerals requires consideration of approximate scattering strengths, and we have not completed experiments to determine how well we will be able to correct for the influence of scattering cross-section.

Pyroxene, plagioclase (now maskelynite) and olivine are the main minerals of EETA 79001, but pyroxene and olivine

Table 1. Representative electron microprobe analyses from EETA79001,442; EETA79001,530 and EETA79001,357[a,b]

	79001,442 (lith A)				79001,530 (lith A)			79001,357 (lith B)							
					ol xenocryst		matrix				px 2				
Thin section	chr	Cr-ulvö	ulvö	ilm	76,[e]	77,[e]	ol	ulvö	ilm	ol[c]	47,[e]	px 2	px 2	merr	Fe-apat[d]
phase	33[e]	12[e]	9[e]	29[e]	rim	core	81[a]	29[e]	33[e]	86[e]	rim	52[e]	57[e]	1720[e]	1718[e]
SiO_2	0.14	0.05	0.06	0.05	36.5	38.6	32.7	0.07	0.07	29.7	50.4	52.3	55.3	0.10	1.96
TiO_2	0.74	16.5	28.1	51.6	0.01	0.01	0.52	28.2	52.0	0.15	0.41	0.45	0.05	<0.01	<0.01
Al_2O_3	7.86	5.04	2.37	0.11	<0.01	0.02	0.09	1.66	0.04	0.01	0.44	1.02	0.21	0.02	0.10
Cr_2O_3	52.8	25.1	5.08	0.27	0.03	0.07	0.10	0.36	0.05	<0.01	0.21	0.33	0.47	n.a	n.a
FeO (total)	31.5	49.3	60.9	45.3	34.6	22.9	52.0	67.6	47.2	66.5	28.8	18.5	16.0	4.97	4.57
MnO	0.43	0.63	0.61	0.67	0.68	0.44	0.62	0.56	0.65	1.10	0.82	0.61	0.53	<0.01	<0.01
MgO	3.22	3.13	1.72	1.66	28.5	37.5	14.9	0.23	0.38	2.14	12.2	13.1	24.4	1.25	0.05
CaO	<0.01	0.08	0.12	0.23	0.28	0.24	0.74	0.01	0.02	0.37	6.68	13.9	2.71	46.2	50.5
Na_2O	n.a	n.a	n.a	n.a	n.a	n.a	n.a	n.a	n.a	n.a	0.08	0.08	0.06	0.72	<0.01
V_2O_3	0.52	0.66	0.42	<0.01	n.a	n.a	n.a	0.07	<0.01	n.a	n.a	n.a	n.a	n.a	n.a
ZnO	0.09	0.11	<0.01	0.04	n.a	n.a	n.a	<0.01	<0.01	n.a	n.a	n.a	n.a	n.a	n.a
NiO	n.a	n.a	n.a	n.a	0.03	0.12	0.14	n.a	n.a	0.01	n.a	n.a	n.a	n.a	n.a
P_2O_5	n.a	n.a	n.a	n.a	n.a	n.a	n.a	n.a	n.a	n.a	n.a	n.a	n.a	45.6	39.2
RE_2O_3[f]	n.a	n.a	n.a	n.a	n.a	n.a	n.a	n.a	n.a	n.a	n.a	n.a	n.a	0.47	0.10
Cl	n.a	n.a	n.a	n.a	n.a	n.a	n.a	n.a	n.a	n.a	n.a	n.a	n.a	<0.01	0.59
F	n.a	n.a	n.a	n.a	n.a	n.a	n.a	n.a	n.a	n.a	n.a	n.a	n.a	0.96	3.31
Sum	97.3	100.6	99.4	99.9	100.6	100.0	101.7	98.8	100.4	100.0	100.1	100.3	99.8	100.3	100.3
—O=F,Cl	—	—	—	—	—	—	—	—	—	—	—	—	—	0.40	1.53
New sum	97.3	100.6	99.4	99.9	100.6	100.0	101.7	98.8	100.4	100.0	100.1	100.3	99.8	99.9	98.8
Mg/(Fe + Mg)					0.59	0.74	0.34			0.05	0.43	0.56	0.73		
Fe/(Fe + Mg)					0.41	0.26	0.66			0.95	0.57	0.44	0.27		
Mt_{xx}[g]		0.098	0.096					0.166							
Wo[h]											16.6	27.7	8.7		
En											35.9	40.4	66.7		
Fs											47.5	31.9	24.5		

[a] More analyses are reported by Wang and co-workers.[6,8]

[b] n.a. = not analyzed; chr = chromite; ulvo = ulvöspinel; ilm = ilmenite; ol = olivine; px = pyroxene; merr = merrillite; apat = apatite.

[c] Olivine in 79001,357 occurs as fayalite in a symplectic intergrowth with px. After accounting for Fe^{3+} the total for chr is close to 97.7% and ulvö to 100%.

[d] Wt% Cl and F indicate apatite although FeO is high; Fe-rich phosphates have been reported previously, e.g. by Steele and Smith.[26]

[e] No. of analyses.

[f] Y, Le, Ce, Nd, Yb measured, other REEs estimated.

[g] Mt_{xx} refers to the calculated magnetite component of the Fe–Ti oxides.

[h] Pyroxene end-member proportions corrected for non-quadrilateral components.

are the major crystalline phases identified in the Raman spectra. Figure 2(a) and (b) show typical spectra of olivine and pyroxene. Crystalline plagioclase, a silicate that has a framework of Si—O bonds, has narrow peaks [Fig. 2(c)] and a fingerprint spectral pattern different from those of olivine (an orthosilicate) and pyroxene (a single-chain silicate) [Fig. 2(a) and (b)]. In addition, variations in peak positions, especially the peaks near 500, 280 and 150 cm^{-1}, can be used to distinguish among different structural and chemical types of feldspars: plagioclase, orthoclase, albite and Na–K feldspar solid solutions (high T and low T structural forms).[9] Spectra for plagioclase are essentially absent from this meteorite, however, because the impact that ejected the rock from the surface of Mars caused a shock wave that converted the plagioclase into maskelynite, and glasses do not give strong Raman spectra. A Raman spectrum of maskelynite is shown in Fig. 2(d), with very broad spectral peaks that are 1–2 orders of magnitude less intense than those of crystalline silicates (olivine, pyroxene, and plagioclase). When maskelynite coexists with any crystalline phases in the area sampled by the excitation laser beam, the Raman signal from maskelynite tends to be masked by the spectral

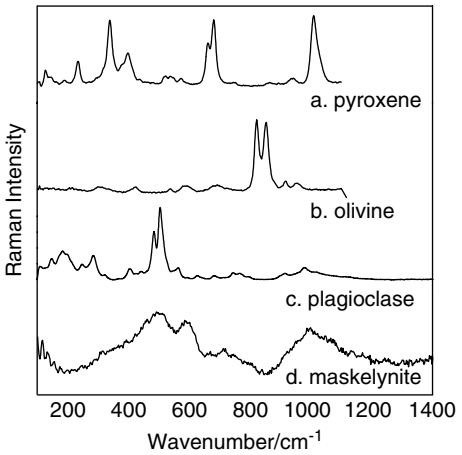

Figure 2. Raman spectra of the major crystalline minerals that make up the meteorite (pyroxene, olivine and feldspar) and maskelynite (feldspar converted to glass by the shock of the meteoroid impact that delivered the meteorite from Mars). Peak intensities are not indicated; those for maskelynite are <0.1 times those of the minerals.

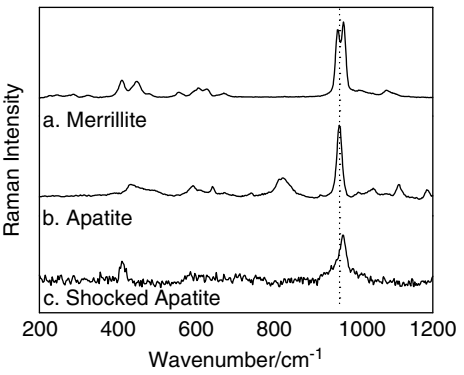

Figure 3. Raman spectra of the three phosphate phases observed in EETA 79001. Merrillite and apatite differ in chemical composition and structure, and therefore spectral signature. Note the peak broadening in the apatite that shows the effects of shock, presumably from the meteoroid impact that ejected the meteorite from Mars.

background of the crystalline phases and is difficult, if not impossible, to extract. Only when the maskelynite grain encountered by the laser beam has a large enough size to fill almost the entire sampling volume (millimeters in diameter, considering the transparent nature of maskelynite), and when its signals is virtually the only contributor to the spectrum, can a definitive identification of this phase be attained, as shown in Fig. 2(d). Considering major mineral proportions on a maskelynite-free basis, we obtained $80 \pm 4\%$ of pyroxene in EETA79001,476 and $82 \pm 4\%$ in EETA79001,482, and $14.1 \pm 1.6\%$ of olivine in EETA79001,476 and $9.5 \pm 1.4\%$ in EETA79001,482. The relative proportions of major crystalline minerals in both rocks are similar to the literature values for lithology A (pyroxene ~84.6–86.7% and olivine ~8.6–12.6% of EETA79001).[21] They are not consistent with the reported mode of lithology B, which has no olivine or chromite.[21]

In addition to the major crystalline silicates (pyroxene and olivine), accessory minerals such as Ca phosphates, Fe oxides and Fe sulfide were also identified, as were some much rarer mineral phases including anatase and calcite. Most accessory minerals have molar proportions <1% in this meteorite, except merrillite. The three phosphate minerals identified by Raman point-counts on rock chips are merrillite, apatite and a shocked form of apatite [Phase A as discovered by Chen *et al*.[23] in shocked SiXiangKou (L6) chondrite]. Electron microprobe data from TS357 (lithology B) suggest Na-merrillite {approximately $Ca_{18}(Fe,Mg)_2(Na,Ca,Mg,REE)[PO_4]_{14}$} and ferroan-fluorapatite {$Ca_{4.7}Fe_{0.3}[PO_4]_3(F_{0.9}Cl_{0.1})$}. Figure 3 shows their mutually distinguishable Raman spectra.

Most opaque minerals, especially Fe-bearing phases, are relatively weak Raman scatterers. The main Fe oxides identified in this meteorite are chromite, magnetite, ulvöspinel and ilmenite; their spectra are shown in Fig. 4. Of the 1065 spectra obtained from 11 point-count traverses on five chips of two rock samples, 39 contain identifiable spectral peaks of Fe–Ti–Cr oxides. We are working towards determining mineral proportions of weak Raman scatters by taking into account the relative Raman cross-sections for common types of minerals (silicates, phosphates, Fe oxides) in volcanic rocks. In an on-surface planetary exploration, obtaining statistically correct proportions of minor minerals will be mainly limited by the number of spectra taken during each Raman point count, which will depend on the mission parameters.

Statistically, the minor and rare phases in a rock would have the same probability of being encountered by a microbeam laser in multi-point measurements (e.g. 100 point linear traverse) as they would under a broad-beam laser in one measurement provided that the total sampling areas are the same. The probability of actually observing the minor and rare phases is greater, however, in a microbeam measurement. That is because the Raman signals from small, rare phases that fall within the condensed beam spot are important contributors to the spectrum at that sampling spot, even when they coexist with the major mineral phases of the rock; their signals are not obscured by those of the major minerals. For example, during a traverse on EETA79001,482, we detected a rare but important alteration mineral in this meteorite, calcite ($CaCO_3$), along with a major mineral, olivine [Fig. 5(a)]. We also detected a few grains of anatase (TiO_2) coexisting with pyroxene [Fig. 5(b)] during two of the traverses.

Pyroxene: compositions and compositional abundance

The major Raman peaks in the spectra of pyroxene (and olivine, see next section) result from the fundamental

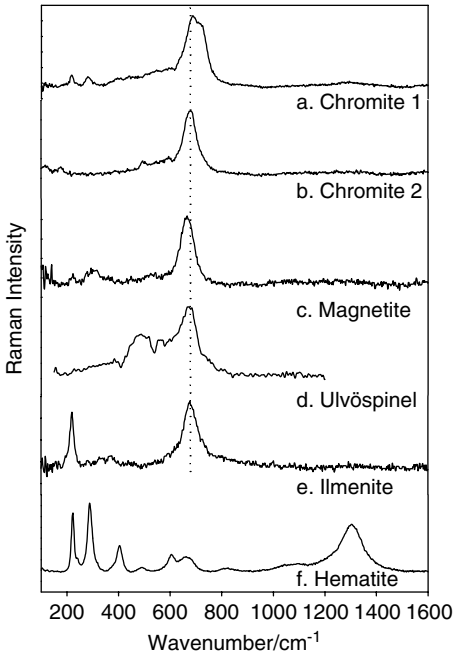

Figure 4. Raman spectra of Fe–Ti–Cr oxides, which occur as minor and trace phases within the meteorite. These phases were mainly produced late in the crystallization of the meteorite from its parent melt as the composition of the residual melt became Fe-rich, and they tend to occur together. The vertical dashed line emphasizes the shifts in position of the peak at ~670 cm^{-1} that result from the different chemical compositions.

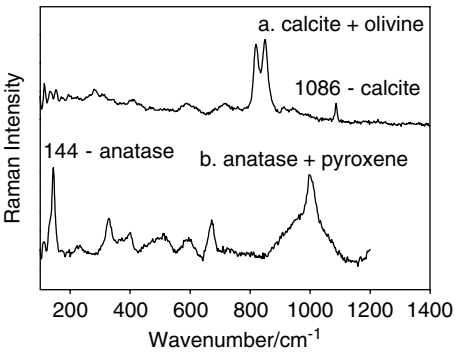

Figure 5. Raman spectra of (a) rare calcite and (b) anatase found on some of the rock chips. The calcite is an alteration mineral that was produced by the action of water and carbon dioxide on the rock after it had crystallized from its parent melt.

vibrations of $[SiO_4]$ tetrahedra and $[Si_2O_7]_n$ chains.[24,25] The different cations (Mg, Fe, Ca, etc.) that occupy the octahedral sites formed by the silicates affect the peak positions of these fundamental vibrations. As a consequence, molar ratios of the major cations in pyroxene and olivine can be determined from their Raman peak positions. The spectra of pyroxene and olivine in EETA79001 rock samples that display extreme peak shifts are shown in Fig. 6(a) and (b).

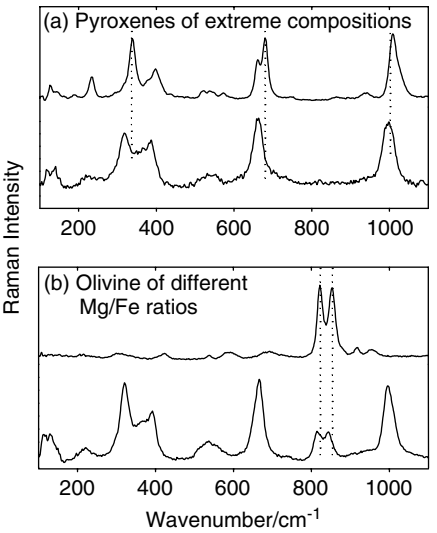

Figure 6. Raman spectra of (a) pyroxene and (b) olivine showing the observed extremes of peak shifts for EETA79001 (marked by dashed line). Part (a) shows an orthopyroxene with $Mg/(Mg + Fe) \approx 0.76$ (top) and a clinopyroxene with $Mg/(Mg + Fe) \approx 0.34$ (bottom). Part (b) shows forsteritic olivine with $Mg/(Mg + Fe) \approx 0.75$ (top) and a fayalitic olivine with $Mg/(Mg + Fe) \approx 0.21$ (bottom) and coexisting with a clinopyroxene with $Mg/(Mg + Fe) \approx 0.43$. Cation ratios are derived from the positions of the peaks.

Correlations have been determined between Raman peak positions and the cation ratios $Mg/(Mg + Fe + Ca)$ and $Ca/(Mg + Fe + Ca)$ for quadrilateral pyroxenes (i.e. pyroxenes in the field of end members $MgSiO_3$, $FeSiO_3$, $MgCaSi_2O_6$ and $FeCaSi_2O_6$).[6] The 1σ accuracy for determining $Mg/(Mg + Fe + Ca)$ values based on Raman data is ~0.06 and for $Ca/(Mg + Fe + Ca) \sim 0.07$. Without spectral curve fitting, the Raman peak position reading error for the laboratory system is about 1 cm^{-1}, which corresponds to a precision of 0.027 for $Mg/(Mg + Fe + Ca)$ values using the correlation between compositions and Raman spectral parameters, as calibrated.

The range of $Mg/(Mg + Fe + Ca)$ ratios of the pyroxene grains in rock samples EETA79001,476 and EETA79001,482 is shown in Fig. 7(a). The similarity in range suggests that the pyroxene grains in these two rock samples are similar compositionally; the continuous and wide range (0.77 to <0.3) is typical of basaltic pyroxene, rapidly crystallized under non-equilibrium conditions. The range of $Mg/(Mg + Fe)$ values calculated on the basis of Raman data is consistent with the published pyroxene data for electron microprobe analyses in the study of Steele and Smith[26] for lithology A2 (the pyroxene–maskelynite matrix of lithology A, i.e. excluding xenocrystic olivine, low-Ca and high-Mg pyroxene and low-Ti chromite megacrysts and crystal clusters). The electron microprobe data published by McSween and Jarosewich[21] [Fig. 2(a)] for lithology A include

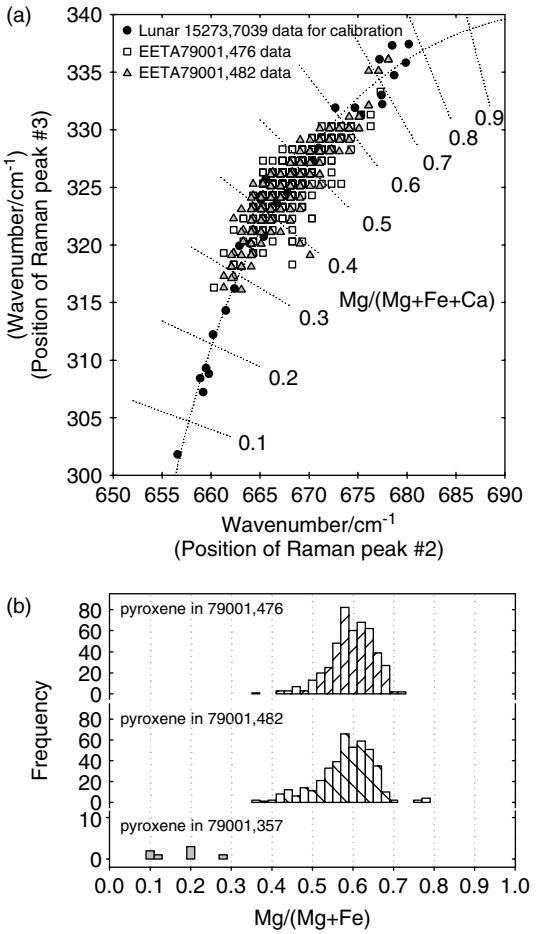

Figure 7. (a) Range of Mg/(Mg + Fe + Ca) in pyroxene of EETA79001,476 and EETA79001,482. The data for pairs of peaks are plotted on a curve that is calibrated for Mg/(Mg + Fe + Ca) using Raman and electron microprobe data for lunar samples.[6] (b) Histograms of compositions of pyroxene in EETA79001,476 rock, EETA79001,482 rock chip, and in thin section EETA79001,357 (lithology B). Information on rock chip cooling history is obtained from the symmetry (or asymmetry) and spread of such mineral compositions.

data for megacrystic pyroxene (which occurs as compound grains with the xenocrystic olivine), so that their range of compositions extends to Mg/(Mg + Fe) > 0.7. We obtained six orthopyroxene spectra whose peak positions indicate the Mg/(Mg + Fe) values >0.7. They all occur in a single, linear traverse separated in two groups. The first occurrence consists of two consecutive spectra with Mg/(Mg + Fe) ~0.76 and the second group consists of four consecutive spectra with Mg/(Mg + Fe) values of 0.75–0.77

The histograms in Fig. 7(b) show the abundance of pyroxene grains of different compositions from the two rock samples (465 pyroxene data points for EETA79001,476 and 420 pyroxene data points for EETA79001,482). Except for the few megacrystic orthopyroxene grains in EETA79001,482, both samples show a unimodal distribution, suggesting a single cooling event, in contrast to, for example, the pyroxene in the Zagami Martian meteorite, which has a complicated cooling history (Fig. 11 in Wang *et al*.[6]). The central portions of both histograms have an essentially Gaussian shape, with peak compositions of Mg/(Mg + Fe) at 0.60. Both histograms show a minor tail at the low side of the Mg/(Mg + Fe) distribution, suggesting some late-stage pyroxene crystallization. The range 0.50–0.70 includes over 96% of the pyroxene in EETA79001,476 and 89% of the pyroxene in EETA79001,482. The distribution of pyroxene compositions in 79001,482 is slightly more skewed to low Mg/(Mg + Fe) than that of 79001,476, which may indicate more rapid crystallization of this portion of the rock.

Olivine: compositions and compositional abundance

Using the Raman spectral data of olivine with known Mg/(Mg + Fe) ratios published by Guyot *et al*.[27] and Chopelas,[28] we developed two correlations to calculate the Mg/(Mg + Fe) molar fraction in olivine (χ^{Mg}) based on the peak positions (ν_1 and ν_2, in cm^{-1}) of the strongest doublet (Fig. 6) (the ~850 cm^{-1} peak and ~820 cm^{-1} peak) in the olivine spectrum:

$$\chi^{Mg} = -830.193 + 1.9017\nu_1 - 0.0010872{\nu_1}^2$$

$$\chi^{Mg} = -2937.162 + 7.0767\nu_2 - 0.0042609{\nu_2}^2$$

The 1σ accuracy for determining Mg/(Mg + Fe) value is ~0.05 using the position of the peak near 850 cm^{-1} and ~0.08 using the position of the peak near ~820 cm^{-1}. Therefore, the position of the ~850 cm^{-1} peak is more suitable for calculating the Mg/(Mg + Fe) for the forsterite–fayalite series. Without doing a spectral curve fit, the 1 cm^{-1} Raman peak position reading error corresponds to a precision of 0.04–0.05 (depending on the position of ~850 cm^{-1} peak). The precision for determining the Mg/(Mg + Fe) cation ratio in olivine is lower than for pyroxene, because the range of Raman peak shifts for olivine is only about half of that for pyroxene.

Figure 8(a) shows the range of Mg/(Mg + Fe) of the olivine grains in rock samples EETA79001,476 and 79001,482. In both samples, the upper limit of the Mg/(Mg + Fe) range (i.e. <0.8) calculated from the Raman data is consistent with the published electron microprobe data for olivine xenocrysts in lithology A1 of Steele and Smith[26] and lithology A of McSween and Jarosewich.[21] Our Raman data reveal minor amounts of Fe-rich olivine not indicated by the two previous studies, however.[21,22] The histograms in Fig. 8(b) show that 7–15% of the data in this study fall outside of the previously reported ranges.[21,22]

The EETA79001,482 rock chips were allocated to us as samples of lithology B. The mineral assemblage revealed by our Raman point-counting measurements is essentially that of lithology A. The pyroxene grains in the rock have a compositional range [Figs. 7(a) and (b)] similar to that

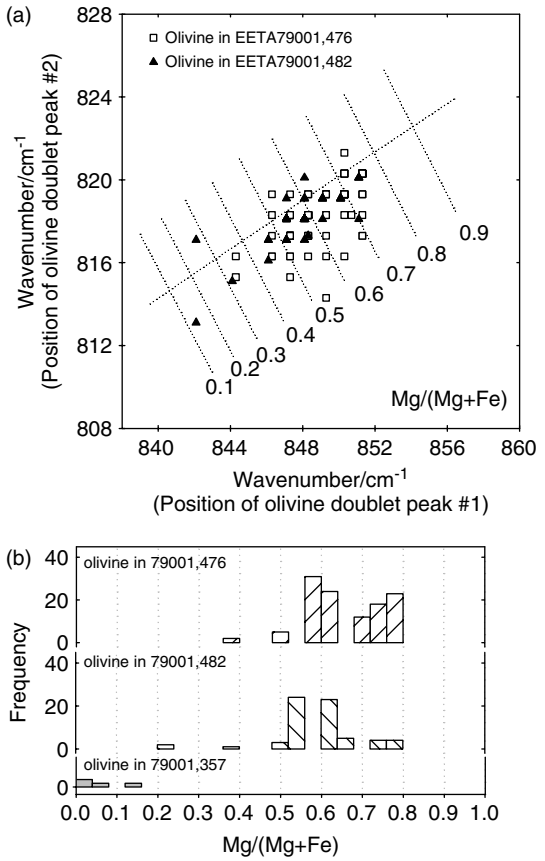

Figure 8. (a) Range of Mg/(Mg + Fe) in olivine of EETA79001,476 and EETA79001,482, shown on a two-peak plot analogous to that of Fig. 7(a). (b) Histograms of compositions of olivine in EETA79001,476 rock, EETA79001,482 rocks, and in thin section EETA79001,357 (lithology B). Three generations of olivine were found in these rock chips.

of EETA79001,476 (a typical sample of lithology A). The compositions of the olivine grains in EETA79001,482 are different from those typical of lithology A, however, as shown in Fig. 8(b). The olivine grains in EETA79001,476 (115 data) have a bimodal distribution, with one group centered at Mg/(Mg + Fe) ≈ 0.7–0.8 and the other at Mg/(Mg + Fe) ≈ 0.6, and a tail of ferroan olivine that extends to Mg/(Mg + Fe) ≈ 0.36. The olivine grains in EETA79001,482 (66 data) have a unimodal distribution centered at Mg/(Mg + Fe) ≈ 0.5–0.6 and a more ferroan tail that extends to Mg/(Mg + Fe) ≈ 0.21. These features, plus the lower mineral proportion of olivine in EETA79001,482 (9.5 ± 1.4% less than 14.1 ± 1.6% of EETA79001, 476), suggest at least a local difference in the crystallization histories of the two rock samples.

Some differences in olivine composition between two of the rock samples can be seen in Fig. 9, which shows the Mg/(Mg + Fe) values of adjacent olivine and pyroxene grains along four linear traverses, two taken on rock sample EETA79001,476 and two others on EETA79001,482. The first traverse in Fig. 9(a) shows pyroxene of the matrix, with randomly distributed Mg/(Mg + Fe) values in the range 0.65–0.55, except for one grain at 0.44. This type of distribution pattern appears in the pyroxene of all the traverses on both rock samples, except two groups of consecutive spectra indicating the Mg/(Mg + Fe) value in the range 0.75–0.77, i.e. megacrystic orthopyroxene. The second traverse in Fig. 9(a) shows a megacryst of olivine surrounded by pyroxene. This olivine grain has a length of ~2 mm and thus yielded 21 consecutive purely olivine spectra (100 μm apart). The central portion of the grain has Mg/(Mg + Fe) ≈ 0.77 and the Mg/(Mg + Fe) decreases gradually at the rims of the grain to ~0.62. The first traverse in Fig. 9(b) reflects the occurrence of an olivine grain of ~0.6 mm length, which yielded 11 continuous spectra (50 μm apart) and a compositional variation from Mg/(Mg + Fe) ≈ 0.60 to 0.50. The second traverse in Fig. 9(b) has two olivine data points that give a very low value of Mg/(Mg + Fe) of ~0.2. The adjacent pyroxene grains also have uncharacteristically low Mg/(Mg + Fe) (0.43), perhaps reflecting a pocket of solidified late-stage melt within the rock.

On the basis of Figs 7–9, we surmise that there are three compositional groups of olivine and two of pyroxene that may represent three stages of crystallization of these EETA79001 rock chips. Coarse, Mg-rich (~Fo_{77}) olivine xenocrysts [Fig. 9(a)] formed (or were incorporated) before the crystallization of pyroxene. The rims of these xenocrysts reacted with the more ferroan host basalt or impact melt and attained equilibrium with the surrounding pyroxene [Fig. 9(a)]. The second type of olivine [Fig. 9(b)] (~Fo_{60}) is in equilibrium with the bulk of the pyroxene in the rock. The components of that olivine type are either smaller grains with initially more magnesian cores that were not sufficiently thick to resist recrystallization, or they are the rims of olivine xenocrysts with the center portion unexposed at the surface that was analyzed. These two types of olivine constitute the bimodal distribution in the histogram of rock chip 79001,476 [Fig. 8(b)]. The third type of olivine [Fig. 9(b), Mg/(Mg + Fe) ≈ 0.21] is ferroan and appears to have formed sparingly from late-stage, residual magma, along with ferroan [Mg/(Mg + Fe) ≈ 0.43] pyroxene, phosphates and opaque phases. The second and third types of olivine constitute the central peak and the ferroan tail, respectively, in the olivine histogram of rock chips 79001,482 [Fig. 8(b)]. This experiment shows how data from Raman traverses (Fig. 9) can show compositional and textural differences.

To verify the existence of olivine in the sample distributed to us as lithology B and to confirm the presence of ferroan olivine, which was not reported by Steele and Smith[26] and McSween and Jarosewich[21] in either lithology A or B, an additional thin section (TS530) was made from one of the rock chips from EETA79001,482. We observed xenocrystic olivine and chromite by electron microprobe analysis and

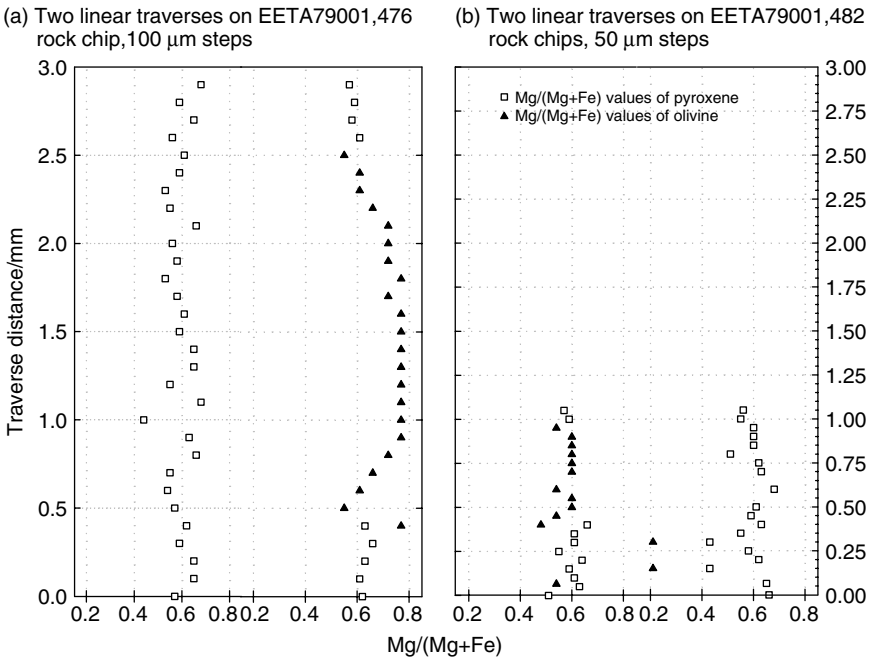

Figure 9. Variations Mg/(Mg + Fe) observed along four linear traverses on EETA79001 rock chips. These variations reflect different conditions of crystallization (see text). Note the relatively high values of Mg/(Mg + Fe) in the core of the large olivine crystal and the compositional zoning to lower Mg/(Mg + Fe) across the rims of the crystal (second traverse).

optical microscopic observation in thin section TS530. The variation of Mg/(Mg + Fe) values of olivine grains in TS530 observed using the electron microprobe [Fig. 10(a)] confirms the existence of three compositional groups as determined by Raman analyses.

In addition, we made detailed Raman measurements on thin section EETA79001,357 (lithology B). Only selected spots in the mesostasis (fine-grained material) were measured, and the olivine and pyroxene data from those spots are displayed in Figs. 7(b) and 8(b). These measurements revealed near end-member fayalite [Mg/(Mg + Fe) < 0.10] coexisting with pyroxferroite also of Mg/(Mg + Fe) < 0.10. These ferroan silicates occur along with phosphates [merrillite and apatite, Fig. 10(b) and (c)] and oxide minerals (ilmenite) that presumably crystallized from the last dregs of residual melt. Using backscattered electron imaging (electron microprobe), we identified a fine-grained interstitial Fe-rich olivine intergrowth with pyroxene in TS357 [Fig. 10(c)], consistent with the Raman data. These Fe-rich olivine and pyroxferroite grains are not associated with the three compositional groups of olivine [Fig. 10(a)] and the pyroxenes found in the rock samples; they are, however, characteristic of lithology B.

On the basis of the olivine compositional features, we conclude that the rock chips of EETA79001,482 may be a mixture of lithologies A and B (olivine and chromite exist in all four of the rock chips). It has been observed previously that although the contact between lithologies A and B is sharp and obvious in some places, elsewhere it is gradational, and in some parts of the meteorite the two lithologies may be more intimately mixed.[29]

Opaque phases in EETA79001

Opaque mineral phases (Fe–Ti–Cr oxides and Fe sulfides) are generally weak Raman scatters. The use of a microbeam system and multipoint measurement procedure increases the probability of their detection and helps to obtain their mineral proportions in a rock.

Iron-bearing sulfide was not detected in the Raman point-count measurements. An Fe sulfide phase was, however, found by our Raman spectroscopic examination in several locations of thin section (TS357, lithology B), where it coexists with ilmenite, titanomagnetite and ulvöspinel. It has a central peak near 290 cm^{-1} and several weak shoulders [Fig. 11(a)]. Compared with well-crystallized sulfides [Fig. 11(b)–(e)], its peaks are broader and thus overlap each other. The position of its Raman peak suggests a solid solution of pyrite, pyrrhotite and troilite, but detailed characterization would require a systematic Raman study of sulfides first. Energy-dispersive electron microprobe analyses showed this phase to be Fe sulfide (we did not analyze it quantitatively to determine Fe–S stoichiometry), which is consistent with the identification as pyrrhotite with a composition of $Fe_{0.93}Ni_{0.03}S$ and $Fe_{0.96}S$.[22]

Among the 1065 spectra obtained from our 11 point-count traverses on five chips of two rock samples, 39 contain identifiable spectral peaks of Fe–Ti–Cr oxides, including chromite, magnetite, ilmenite and ulvöspinel (most of them are solid solutions). Typical Raman spectra obtained from Fe–Ti–Cr oxides in the point-counting measurements on the rock chips are shown in Fig. 4. Among them, chromite has a coarse grain size, as shown by its occurrence in spectra

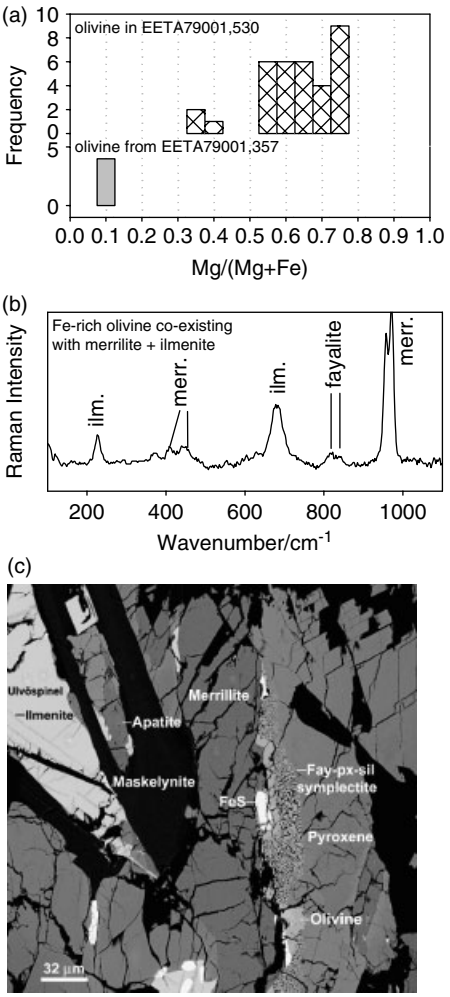

Figure 10. (a) EMPA data on Mg/(Mg + Fe) of olivine grains in thin sections TS530 and TS357. (b) Raman spectrum of an Fe-rich olivine crystal that coexists with merrillite and ilmenite. Such intergrowths occur in small pockets of residual melt late in the crystallization sequence of the rock. (c) Backscattered electron image showing fayalite–pyroxene–silica symplectite (intergrowth).

from as many as three consecutive points (100 μm apart) in a linear traverse. The major Raman peak of chromite from this meteorite occurs in a range from 679 to 699 cm^{-1} [Fig. 4(a) and (b)], which corresponds to a $(Cr + Fe^{3+})/(Cr + Fe^{3+} + Al)$ ratio of 0.75–1.0.[8] Although not reported in previous studies on EETA79001, magnetite was detected in Raman point-counting measurements on EETA79001,482 rock chip [Fig. 4(c)]. Magnetite and ulvöspinel [Fig. 4(d)] found in this meteorite have smaller grain sizes, are always observed in multi-phase spectra and only rarely appear in sequential spectra. The positions of their major peaks are not very sensitive to the Fe/Ti ratio in the structure; however, a general classification can be made to separate the near end-member magnetite from magnetite–ulvöspinel solid solutions. The Raman peak positions [Fig. 4(e)] of ilmenite

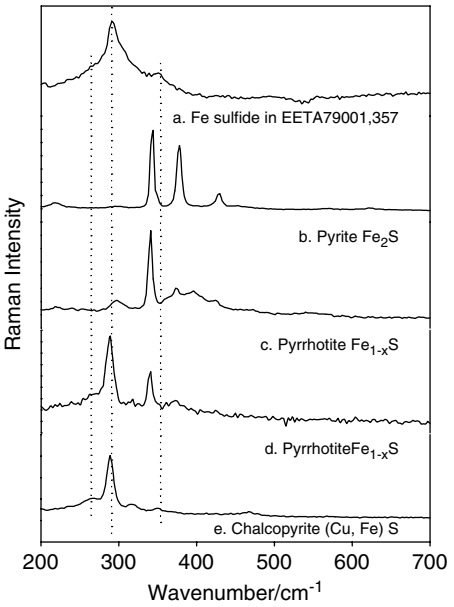

Figure 11. Typical spectrum of Fe sulfide found in EETA79001,357 compared with those of reference Fe sulfides. Note the broader peaks of the EETA sulfide, indicative of poorer crystallization and possible intimate mixing of more than one sulfide phase.

grains found in the rock chips of this meteorite are at or below 680 cm^{-1}, which suggests Ti/Fe ratios near 1.0 and Mg/(Mg + Fe) ratios near 0.[8] These values are consistent with the electron microprobe measurements on ilmenite grains that we found in both thin sections, EETA79001,442 and 79001,357 (Table 1). In the light of the fact that magnetite has not been reported previously in EETA79001 (other than some early references to ulvöspinel as titanomagnetite) and our own electron probe analyses have encountered only titanomagnetite, thus we infer that the Raman spectra represent titanomagnetite.[8]

Hematite has not previously been reported in EETA79001.[21] One spectrum [Fig. 4(f)] from rock chip, 79001,482 shows peaks of end-member hematite and has characteristic spectral features for well-crystallized hematite, i.e. all of the fundamental vibration peaks are present, the peaks are sharp and the S/N ratio is high. This suggests that hematite may be a rare but original phase in this meteorite. That would indicate the development of a highly localized oxidizing environment on a microscopic scale.

CONCLUSION

Correlated laser Raman and electron microprobe analyses demonstrate that significant information regarding the mineral modes and major compositional features of the main mineral groups in EETA79001 can be obtained from Raman point-count measurements, especially traverse across sections of cut and rough, unprepared surfaces. A basic

petrological understanding of a rock such as EETA79001 can be achieved by combining information on coexisting mineral phases, mineral modes, and rock textures for different lithologies, all obtained from the same set of Raman point-counting measurements across.

Acknowledgements

We thank the thin section laboratory at JSC for their excellent work and we thank the Meteorite Working Group (MWG) for allocation of samples of EETA79001 for Raman spectroscopic study. This work was supported in part by NASA grants NAG5-10703, NAG5-12114 and NAG5-12684.

REFERENCES

1. Garvin JB, McCleese DJ. In *6th International Conference on Mars*. 2003; 3177. http://www.lpi.usra.edu/meetings/sixthmars2003/pdf/3177.pdf.
2. Chicarro AF. In *6th International Conference on Mars*. 2003; 3049. http://www.lpi.usra.edu/meetings/sixthmars2003/pdf/3049.pdf.
3. Wang A, Haskin LA, Lane AL, Wdowiak TJ, Squyres SW, Wilson RJ, Hovland LE, Manatt KS, Raouf N, Smith CD. *J. Geophys. Res.* 2003; **108**(E1): 5005. doi:10.1029/2002JE001902.
4. Wang A, Jolliff BL, Haskin LA. *J. Geophys. Res.* 1999; **104**: 8509.
5. Wang A, Jolliff BL, Haskin LA. *J. Geophys. Res.* 1999; **104**: 27 067.
6. Wang A, Jolliff BL, Haskin LA, Kuebler KE, Viskupic KM. *Am. Mineral.* 2001; **86**: 790.
7. Wang A, Freeman J, Kuebler KE. In *Lunar and Planetary Science Conference XXXII*. 2002; 1374.
8. Wang A, Kuebler KE, Jolliff BL, Haskin LA. *Am. Mineral.* 2004; (In press).
9. Freeman J, Wang A, Kuebler KE, Haskin LA. In *Lunar and Planetary Science Conference XXXIV*. 2003; 1676.
10. Haskin LA, Wang A, Rockow KM, Jolliff BL, Korotov RL, Viskupic KM. *J. Geophys. Res.* 1997; **102**: 19 293.
11. Kuebler KE, Wang A, Haskin LA, Jolliff BL. In *Lunar and Planetary Science Conference XXXIV*. 2003; 1953.
12. Wang A, Haskin LA, Gillis JJ. In *Lunar and Planetary Science Conference XXXIV*. 2003; 1753.
13. Wang A, Haskin LA, Kuebler KE, Jolliff BL, Walsh MM. In *Lunar and Planetary Science Conference XXXII*. 2001; 1423.
14. Wang A, Kuebler KE, Freeman J, Jolliff BL. In *Lunar and Planetary Science Conference XXXII*. 2001; 1431.
15. Wang A, Jolliff BL, Haskin LA. In *6th International Conference on Mars*. 2003; 3270. http://www.lpi.usra.edu/meetings/sixthmars2003/pdf/3270.pdf.
16. Haskin LA, Wang A. In *Lunar and Planetary Science Conference XXXIV*. 2003; 1651.
17. Hunten DM, Pepin RO, Walker JCG. *Icarus* 1987; **69**: 532.
18. Bogard DD, Johnson P. *Science* 1983; **221**: 651.
19. Becker RH, Pepin RO. *Earth Planet. Sci. Lett.* 1984; **69**: 225.
20. Ott U, Begemann F. *Nature* 1985; **317**: 509.
21. McSween HY Jr, Jarosewich E. *Geochim. Cosmochim. Acta* 1983; **47**: 1501.
22. Mittlefehldt DW, Lindstrom DJ, Lindstrom M, Martinez RR. *Meteorit. Planet. Sci.* 1999; **34**: 357.
23. Chen M, Wopenka B, Xie X, El Goresy A. In *Lunar and Planetary Science Conference XXVI*. 1995; 237.
24. Iishi K. *Am. Mineral.* 1978; **63**: 1198.
25. Dele-Dubois ML, Dhamelincourt P, Schubnel HJ. *Revue de Gemm. A.F.G.* 1980; **64**: 11, 13–16.
26. Steele IM, Smith JV. In *Lunar and Planetary Science Conference XIII, Part 1, JGR Suppl*. 1982; **87**: A375.
27. Guyot F, Boyer H, Madon M, Velde B, Poirier JP. *Phys. Chem. Mineral.* 1986; **13**: 91.
28. Chopelas A. *Am. Mineral.* 1991; **76**: 1101.
29. Meyer C. *JSC Report 27672*. Johnson Space Center: Houston, Tx, 1996; 43–50 67–90.